**Structure–deactivation relationships in zeolites during the methanol-to-hydrocarbons reaction: Complementary assessments of the coke content**

# Structure–deactivation relationships in zeolites during the methanol–to-hydrocarbons reaction: complementary assessments of the coke content

Daniel Rojo-Gama[a], Matteo Signorile[c], Francesca Bonino[c], Silvia Bordiga[c], Unni Olsbye[a], Karl Petter Lillerud[a], Pablo Beato[b], Stian Svelle[a]

[a]Center for Materials Science and Nanotechnology (SMN), Department of Chemistry, University of Oslo, P.O. Box 1033, Blindern, N-0315 Oslo, Norway

[b]Haldor Topsøe A/S, Haldor Topsøes Allé 1, 2800 Kgs. Lyngby, Denmark

[c]Department of Chemistry, NIS and INSTM Reference Centre, University of Turin, Via G. Quarello 15, I-10135 and Via P. Giuria 7, I-10125, Turin, Italy

Corresponding authors:

Professor Stian Svelle

e-mail: stian.svelle@kjemi.uio.no

Phone: +47 22 85 54 54

Dr. Pablo Beato

e-mail : pabb@topsoe.dk

Phone: +45 45 27 20 00

# Supplementary Material

## S.1. Catalyst structures

- MOR (Mordenite) zeolite has 12- and 8-membered ring channels distributed parallel to the c-axis. These systems are connected by 8-ring channels parallel to the b-axis. Channel dimensions are 6.5 Å x 7.0 Å and 5.7 Å x 2.6 Å for the 12- and 8-membered rings, respectively [1]. The eight rings are not accessible to any diffusing species. The perpendicular eight-ring channels that run in the b-direction are very tortuous, leading to the so-called side pockets to the 12 rings. Thus, molecules are unlikely to pass through the eight rings because of steric limitations. Mordenite is in real terms, a one-dimensional 12-ring system.

- TON (ZSM-22) is a one-dimensional 10-ring zeolite. The 10-ring channels are elliptical and slightly zigzag in shape with dimensions 5.7 Å × 4.6 Å. The maximum diameter of a sphere that can be included in the channels of ZSM-22 is 5.71 Å [1].

- MFI (ZSM-5): ZSM-5 is a three-dimensional medium pore zeolite made from interconnecting straight and sinusoidal 10-ring channels. The straight channels have dimensions of 5.3 × 5.5 Å and the sinusoidal ones 5.4 Å × 5.6 Å. The maximum diameter of a sphere that can be fitted in the channels of ZSM-5 is 6.36 Å [1].

- *BEA (Beta) zeolite is a disordered structure made of three intergrown polymorphs A, B, and C [2]. Polymorphs have a three-dimensional 12-ring channel. Polymorphs are individually ordered, but the stacking produce a disordered structure along the c-axis. All polymorphs have two linear channel systems, mutually orthogonal and perpendicular to the c-axis. These two linear channels intersect producing a third channel system, parallel to the c-axis and with sinusoidal shape. Linear channels have the dimensions 6.6 Å x 7.7 Å. and the third channel, highly tortuous is smaller with dimensions of 5.6 Å x 5.6 Å [1].

- CHA (SAPO-34) is a zeotype material having the chabazite topology with a three dimensional small pore structure, made of Si Al and P as T-atoms. The pore system in SAPO-34 catalyst is formed by large cages constructed by 12 ring openings that are connected with 8-ring windows of 3.8 Å × 3.8 Å dimensions. The maximum diameter of a sphere that can be included in the cages of SAPO-34 is 7.37 Å [1].

**Table S.1.** Key structural data for the catalysts employed

| Topology | Channel dimensionality | Ring size(s) | Channel dimensions |
|---|---|---|---|
| MOR (Mordenite) | 1D | 12 (with 8R side pockets)<br>8 (closed for diffusion) | 6.5 × 7.0 Å and 2.6 × 5.7 Å |
| TON (ZSM-22) | 1D | 10 | 4.6 × 5.7 Å |
| MFI (ZSM-5) | 3D | 10 | 5.1 × 5.5 Å and 5.3 × 5.6 Å |
| *BEA polymorph A (Beta) | 3D | 12 | 5.6 × 5.6 Å and 6.6 × 6.7 Å |
| CHA (SAPO-34) | 3D, cavity based | 8 | 3.8 × 3.8 Å |

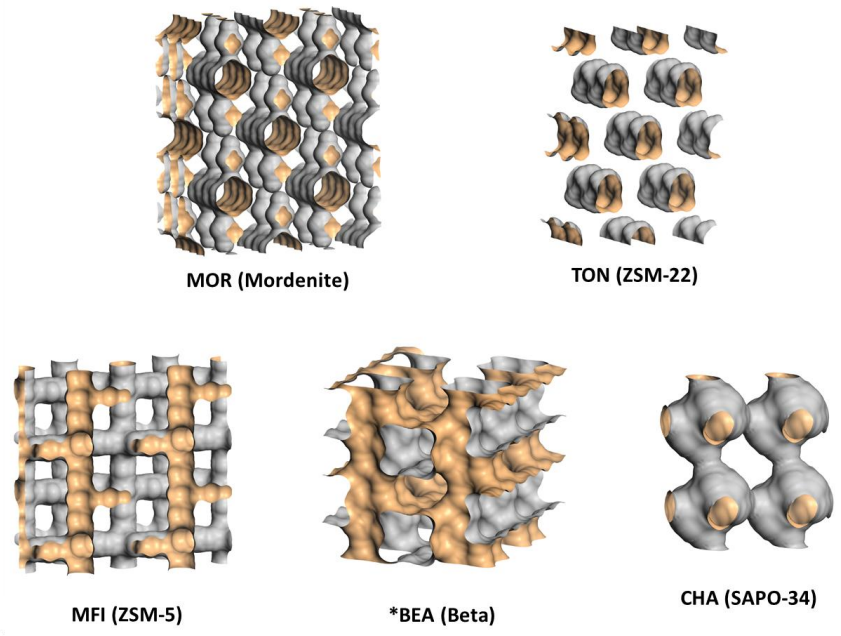


**Figure S.1** Schematic view of the pore systems of the catalysts used in this study.

## S.2. General catalyst characterization

Figure S.2 shows the diffractograms of the 5 different samples used in this study. Blue curves represent the experimental data, the red curves show the diffractograms using Le Bail refinement, and the difference between the experimental and the refined values is depicted in black. According to the results, all samples display their crystallinity and high purity. It is worthwhile noting that in the case of Beta, the differences between experiment and simulation are the largest, due to the fact that beta is made of 3 different polymorphs that are not considered in the model. Moreover, the peak broadening is additionally assigned as the small particle size of this material.

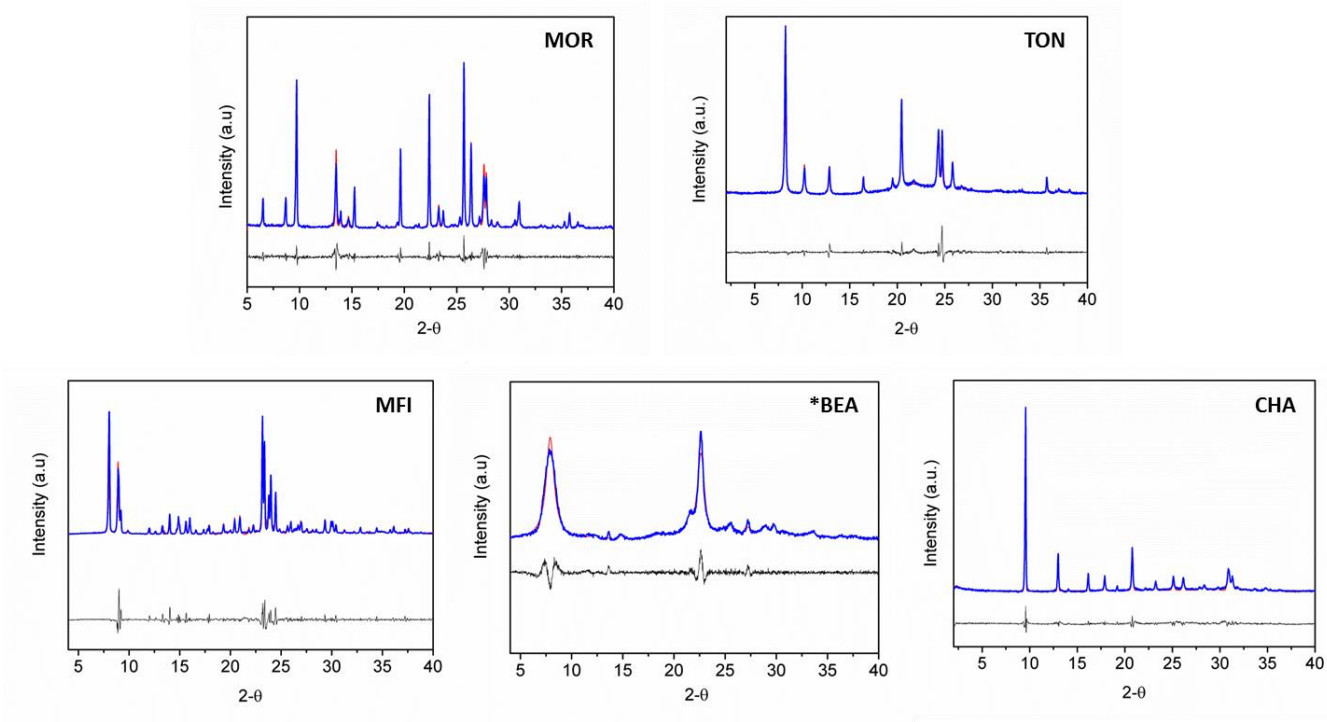


**Figure S.2.** Powder XRD full-profile data with Le Bail refinement. In each sample, the blue line represents the experimental data, red the model refined, and the difference between them is shown in black.

SEM images shown in Figure S.3 show the particle size and shape of the different zeolites used. As observed, Mordenite displays agglomeration of crystals in the 2-6 µm range. ZSM-22 shows its typical needle-like shape with crystallites in the range of 2-5 µm. ZSM-5 shows crystals with sizes between 1–4 µm and prismatic shape. The Beta sample is characterized by having very small crystals which agglomerate in larger units. Finally, the micrograph of SAPO-34 displays crystals with cubic structure and size smaller than 1 µm.

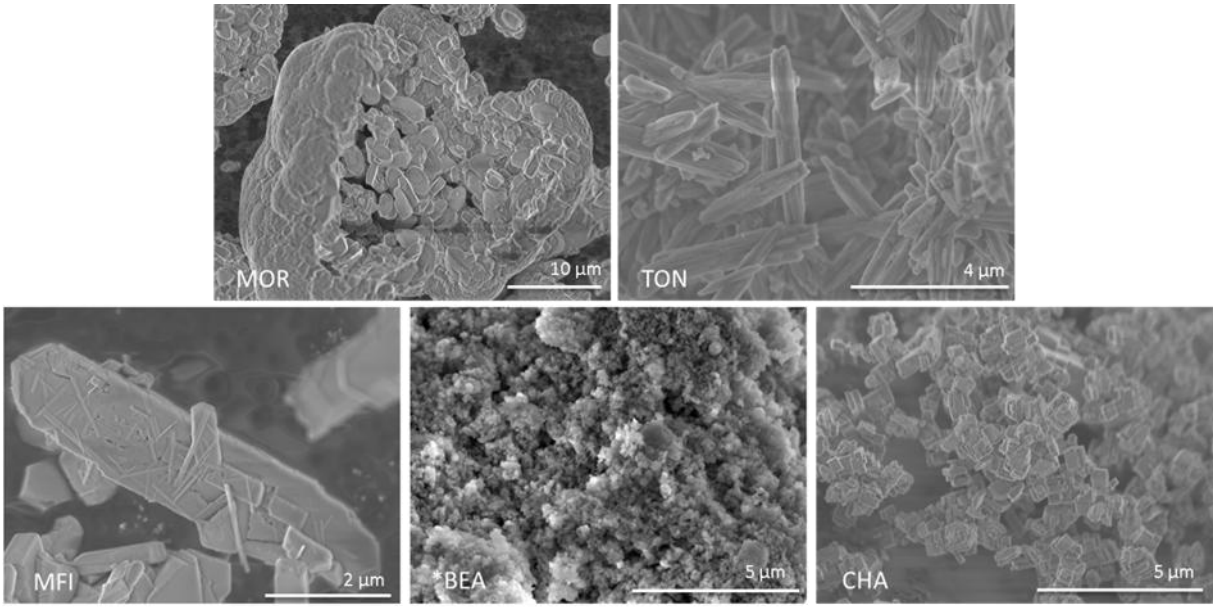


**Figure S.3.** Scanning electron micrographs of the catalysts used.

$N_2$ adsorption isotherms for the five different catalysts are shown in Figure S.4. Mordenite, ZSM-5 and SAPO-34 display a type I isotherm, with high nitrogen uptake at relative low pressures, a feature characteristic of purely microporous samples. Similarly, ZSM-22 also shows a high uptake of nitrogen at low partial pressures, as a clear evidence of the micro porosity of the material. Even though there is a hysteresis effect in the desorption for ZSM-22 that might be interpreted as a certain degree of mesoporosity, it has been discussed [3, 4] that this hysteresis effect is associated to a phase transition of the adsorbed nitrogen from a disordered state to a more order phase, concluding that no mesoporosity was detected in this material. Finally Beta shows an isotherm type IV, where there are two clear steps in the nitrogen uptake. This is typical of materials where several adsorbate layers are formed and where the heat of adsorption of the first layer is different compared to the next layers.

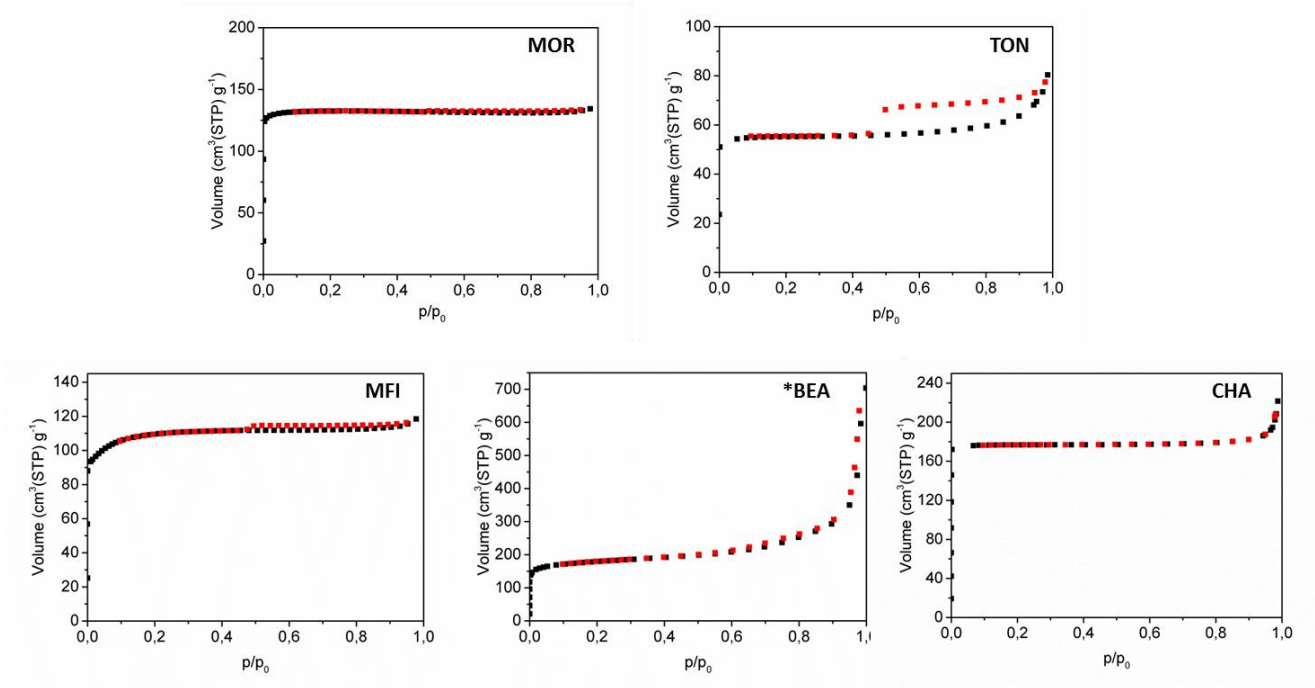


**Figure S.4.** $N_2$ adsorption (black) and desorption (red) isotherms on the different catalysts used. Black symbols correspond to the adsorption isotherm and red symbols to the desorption isotherm.

As shown in Table S.2, with the exception of Beta zeolite, the micropore volume for fresh catalysts does not show large differences with respect the method used for its determination. The fact that adsorption isotherm in Beta does not reach a horizontal plateau at $p/p_0$ = 0.2 is the source of the dissimilarity in micropore volume.

**Table S.2.** Comparison of micropore volume values for fresh catalysts determined either by the $N_2$ uptake at $p/p_0$ = 0.2 or the t-plot method.

| Catalyst | Micropore volume (From the uptake $N_2$ at $p/p_0$ 0.2) | Micropore volume (t-plot) |
|---|---|---|
| Mordenite | 0.19 | 0.20 |
| ZSM-22 | 0.08 | 0.08 |
| ZSM-5 | 0.17 | 0.16 |
| Beta | 0.20 | 0.27 |
| SAPO-34 | 0.27 | 0.27 |

The top graph of Figure S.5 shows the FTIR spectra of Mordenite upon interaction of CO. The left panel represents the hydroxyl stretching region and the right panel shows the CO stretching region. The spectrum of the dehydrated zeolite is shown in red and the spectrum at the highest CO loading is shown in blue.

In Mordenite, Brønsted sites are shifted from 3160 $cm^{-1}$ to 3300 $cm^{-1}$ and the silanol band from 3747 $cm^{-1}$ to 3645 $cm^{-1}$. A shoulder at ~3580 $cm^{-1}$ is due to terminal silanols. In the CO stretching region, the band for CO interacting with Brønsted sites is observed at 2176 $cm^{-1}$ whereas for the CO adsorbed on silanols, the band is observed at 2155 $cm^{-1}$. A weak band at ~2230 $cm^{-1}$ is observed, assigned to CO adsorbed on strong Lewis sites, ascribed in the literature to highly uncoordinated $Al^{3+}$ [5-8]. Additionally, the band at 2135 $cm^{-1}$ is assigned to CO physically adsorbed. The qualitative picture offered by CO adsorption is confirmed by pyridine, where the clear signals at 1545 $cm^{-1}$ and 1454 $cm^{-1}$ (ascribed to the interaction with Brønsted and Lewis sites respectively) are observed.

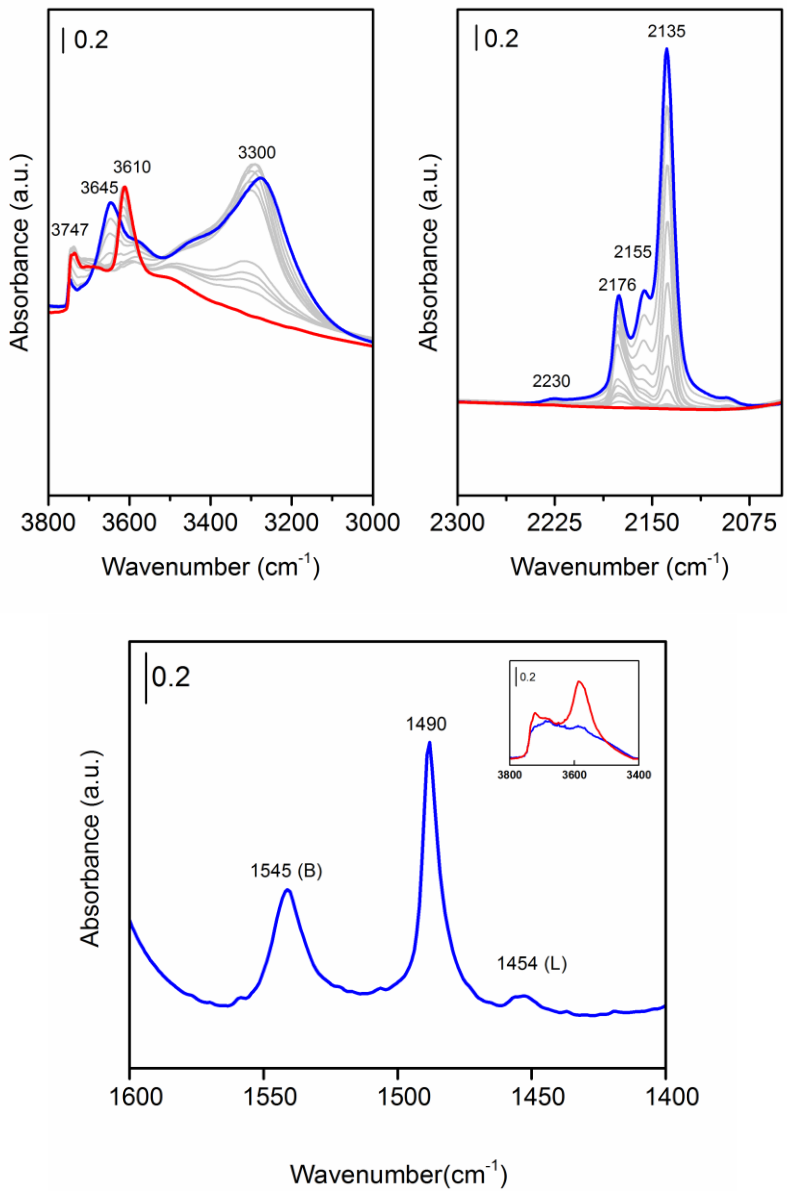


**Figure S.5.** Top: FTIR spectra of Mordenite catalyst upon interaction with CO in the OH region (left) and in the CO region (right). Bottom: FTIR spectrum of Mordenite upon interaction of pyridine and subsequent heating at 200 °C for two hours.

The red spectra shown in the top panel of Figure S.6 corresponds to the dehydrated ZSM-22 whereas the spectrum measured at the highest loading of CO is depicted in blue. Silanol and Brønsted acid site peaks are observed at 3744 $cm^{-1}$ and 3603 $cm^{-1}$, respectively. The silanol band is asymmetric, with a tail towards the lower wavenumbers which is associated to different silanol groups. The isolated silanols are shown by the sharp peak at 3744 $cm^{-1}$ while the tail is due to terminal silanols. Upon CO adsorption, hydroxyl groups were perturbed. It is observed that bridging Brønsted acid sites band at 3603 $cm^{-1}$ erodes while a new band at 3280 $cm^{-1}$ appears.

As hydroxyls groups are perturbed, new bands appear in the CO region. CO forms hydrogen bond with bridging Brønsted acid sites, and the ν(CO) band is shown at 2174 $cm^{-1}$.

After all Brønsted acid sites were totally consumed, silanol groups started to get consumed. The silanol band at 3744 $cm^{-1}$ was eroded to lower wavenumber, 3650 $cm^{-1}$. It is noteworthy that the decrease in silanol band is very smooth. At the same time, CO adsorbed on silanols displays a shift to 2155 $cm^{-1}$. The band at 2137 $cm^{-1}$ is assigned to CO physically adsorbed in the zeolite channels [5].

No clear evidences of strong Al Lewis acid sites (isolated $Al^{3+}$ giving the 2230 $cm^{-1}$ band) are recognized upon CO adsorption. Conversely the presence of clusterized alumina like extraframework Al, giving rise to lower shifts of the CO stretching mode (e.g. 2195 $cm^{-1}$ for oxide-like tricoordinated Al, or even 2153 $cm^{-1}$ in presence of a bulk alumina phase) cannot be excluded as such frequencies are overlapping with the major features of the CO interacting with the Brønsted sites [7, 8].

Bottom panel shows the interaction of pyridine with ZSM-22 collected after evacuation of its physisorbed fraction at 200 °C for 2 hours. All Brønsted sites were consumed upon interaction with pyridine as depicted by the inset in the graph. Interestingly, this stronger basis is able to demonstrate the presence of a small amount of Lewis sites, as the 1455 $cm^{-1}$ peak is observed. In this case, the combination of results from pyridine and CO adsorption suggests the absence of highly uncoordinated $Al^{3+}$. A satellite peak of the 1455 $cm^{-1}$ is further observed at 1440 $cm^{-1}$ and can be assigned to residual physisorbed pyridine [9, 10], still present due to the remarkable diffusion limitation proper of the ZSM-22 topology. From this experimental result, quantification of Brønsted and Lewis acid sites is performed.

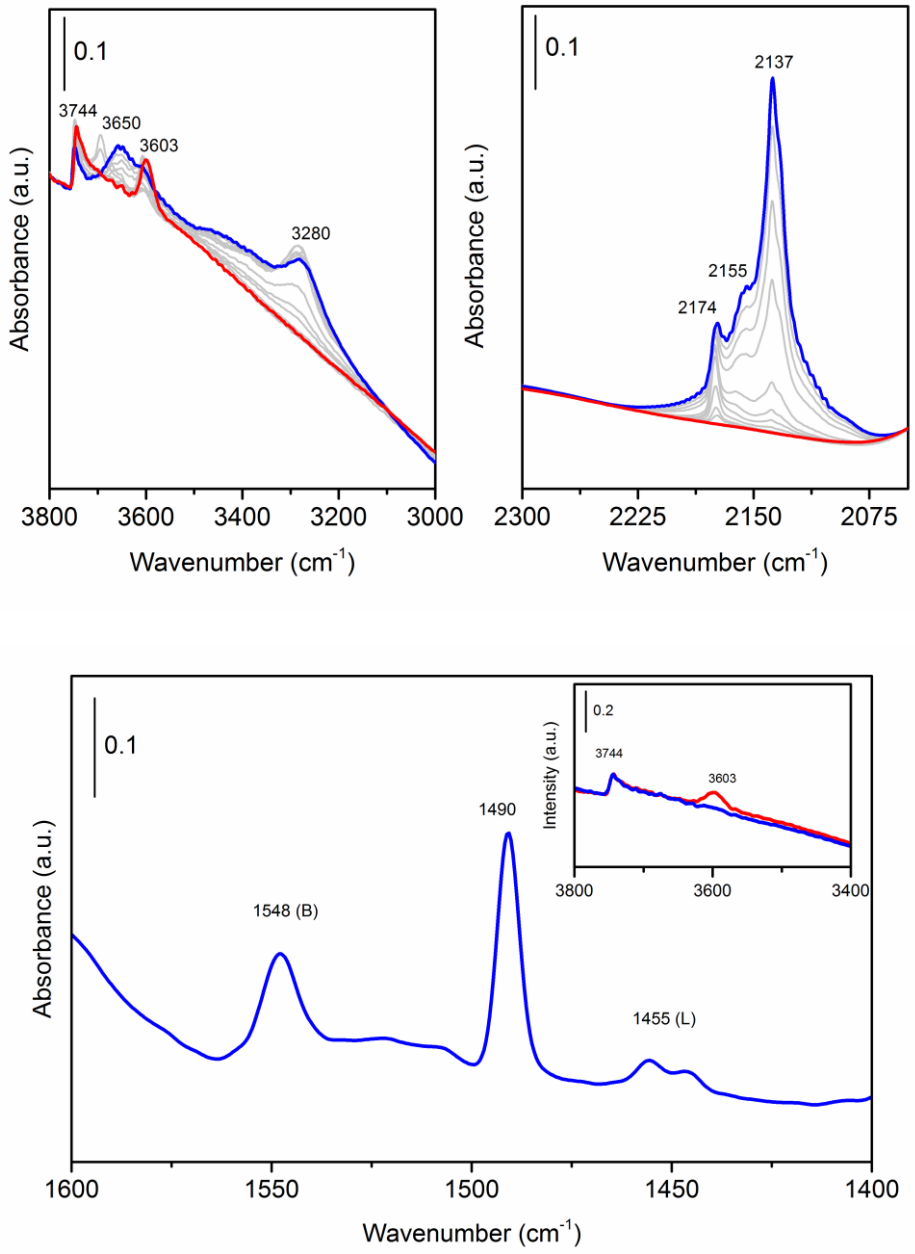


**Figure S.6.** Top: FTIR spectra of ZSM-22 catalyst upon interaction with CO in the OH region (left) and in the CO region (right). Bottom: FTIR spectra of ZSM-22 upon interaction of pyridine and subsequent heating at 200 °C for two hours.

As in previous materials, the top panel of Figure S.7 shows the interaction of CO with the zeolite and the bottom graph the interaction with pyridine. The red spectrum corresponds to the dehydrated and activated zeolite and the blue one at the highest CO loading. Results of this ZSM-5 sample show that very little amount of silanols, represented at 3745 $cm^{-1}$, are detected, but large amount of Brønsted sites are observed 3607 $cm^{-1}$. Upon CO adsorption the Brønsted band is shifted to 3279 $cm^{-1}$ and the corresponding CO stretching mode is observed at 2172 $cm^{-1}$.

As the intensity of the original silanol band is very weak, the perturbation band is hardly detected at ~3620 $cm^{-1}$ in the OH stretching region. In this particular zeolite, there is no band detected around 2155 $cm^{-1}$ associated to CO adsorbed on silanols due to the very little amount of these sites detected in the dehydrated material. Concerning the detection of Lewis sites, as previously commented for ZSM-22, CO adsorption excludes the presence of highly uncoordinated $Al^{3+}$. However, the existence of other kind of Lewis sites (see above), can be inferred on the basis of the pyridine adsorption experiments that show a clear component at 1455 $cm^{-1}$.

The latter is reported in the bottom panel of Figure S.7: the spectrum obtained after evacuation for 2 hours at 200 °C is reported. The inset in the graph shows a total consumption of Brønsted sites. Finally, with the area obtained for the different acid sites, a quantification of the Brønsted and Lewis sites was performed.

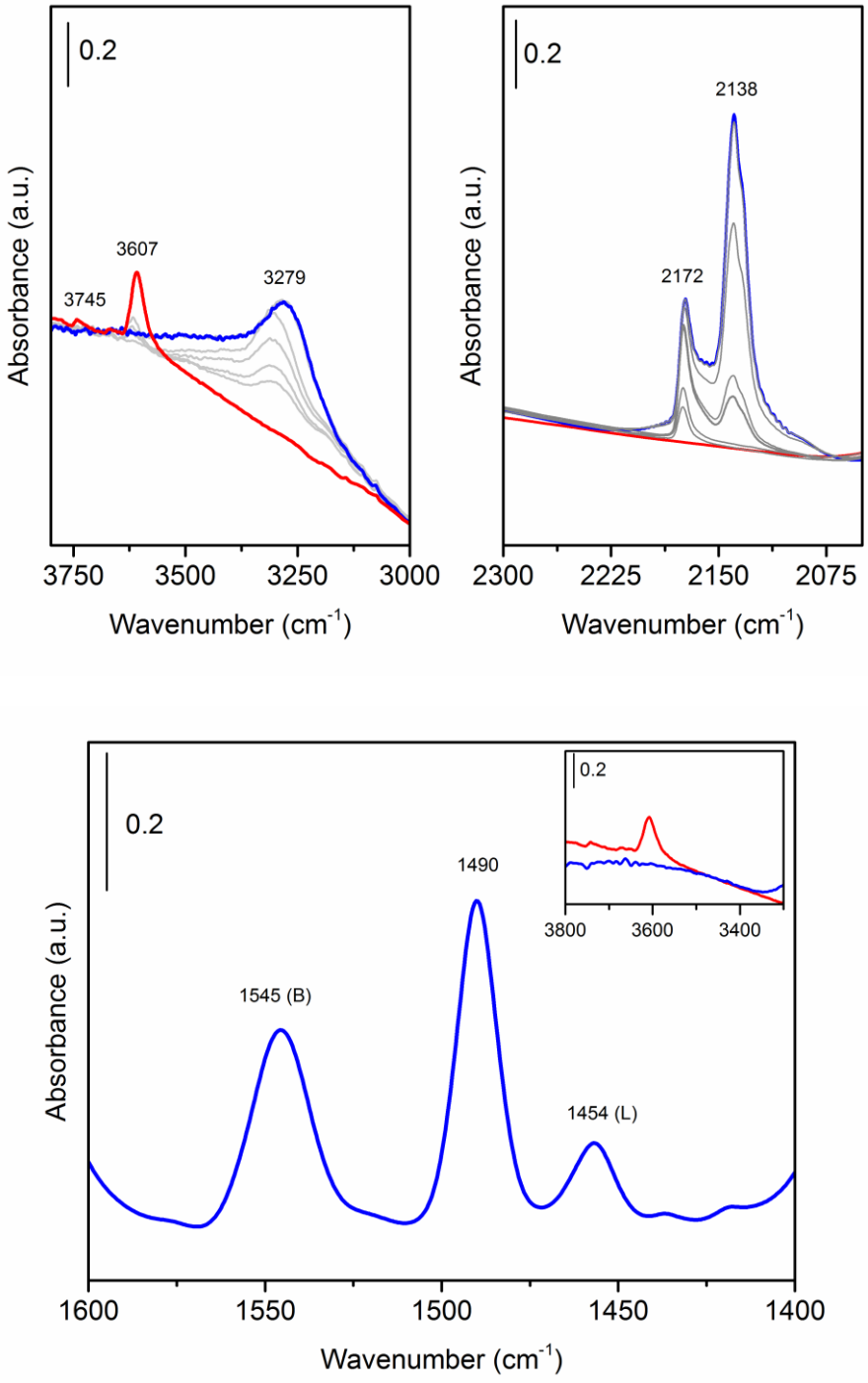


**Figure S.7.** Top: FTIR spectra of ZSM-5 catalyst upon interaction with CO in the OH region (left) and in the CO region (right). Bottom: FTIR spectra of ZSM-5 upon interaction of pyridine and subsequent heating at 200 °C for two hours.

The red spectrum on the top graph of Figure S.8 corresponds to the dehydrated Beta zeolite. The intensity of the silanol band at 3749 $cm^{-1}$ obtained in Beta is much higher than the band associated to Brønsted sites at 3607 $cm^{-1}$. This high intensity of the silanol band can be expected for zeolites with small particle size, as it is the case in this Beta sample, where there is a larger external surface (i.e. more isolated silanols) with respect to the bulk. A further signal detected at 3782 $cm^{-1}$ clearly suggests the presence of Al-OH groups of a bulk alumina phase[11].

When CO was dosed, the stretching vibration of Brønsted sites was shifted to 3296 $cm^{-1}$ whereas the silanols were shifted to 3650 $cm^{-1}$. CO adsorbed on Brønsted sites are observed at 2172 $cm^{-1}$ while interaction of CO with silanols is reflected by the band at 2160 $cm^{-1}$. The vibration at 2138 $cm^{-1}$ is assigned to CO physisorbed in the zeolite channels, and the band at ~2230 $cm^{-1}$ is assigned to the interaction of CO with strong Lewis sites. The appearance of a small component at 2230 $cm^{-1}$ tailed towards lower wavenumbers, suggests the presence of both highly uncoordinated $Al^{3+}$ and oxide-like tricoordinated Al Lewis sites.

Upon adsorption of pyridine, observed in the bottom panel, the inset graph shows that all the Brønsted sites were consumed, but the decrease in the silanol band was not complete. Conversely the small peak at 3782 $cm^{-1}$ is totally consumed upon interaction. After evacuation for 2 hours at 200 °C, the spectrum observed in allowed to quantify the different acid sites. In this last case, the pyridine ring stretching region evidences the particularly strong contribution due to the Lewis sites, confirming the presence of both isolated $Al^{3+}$ uncoordinated sites and extended alumina phases.

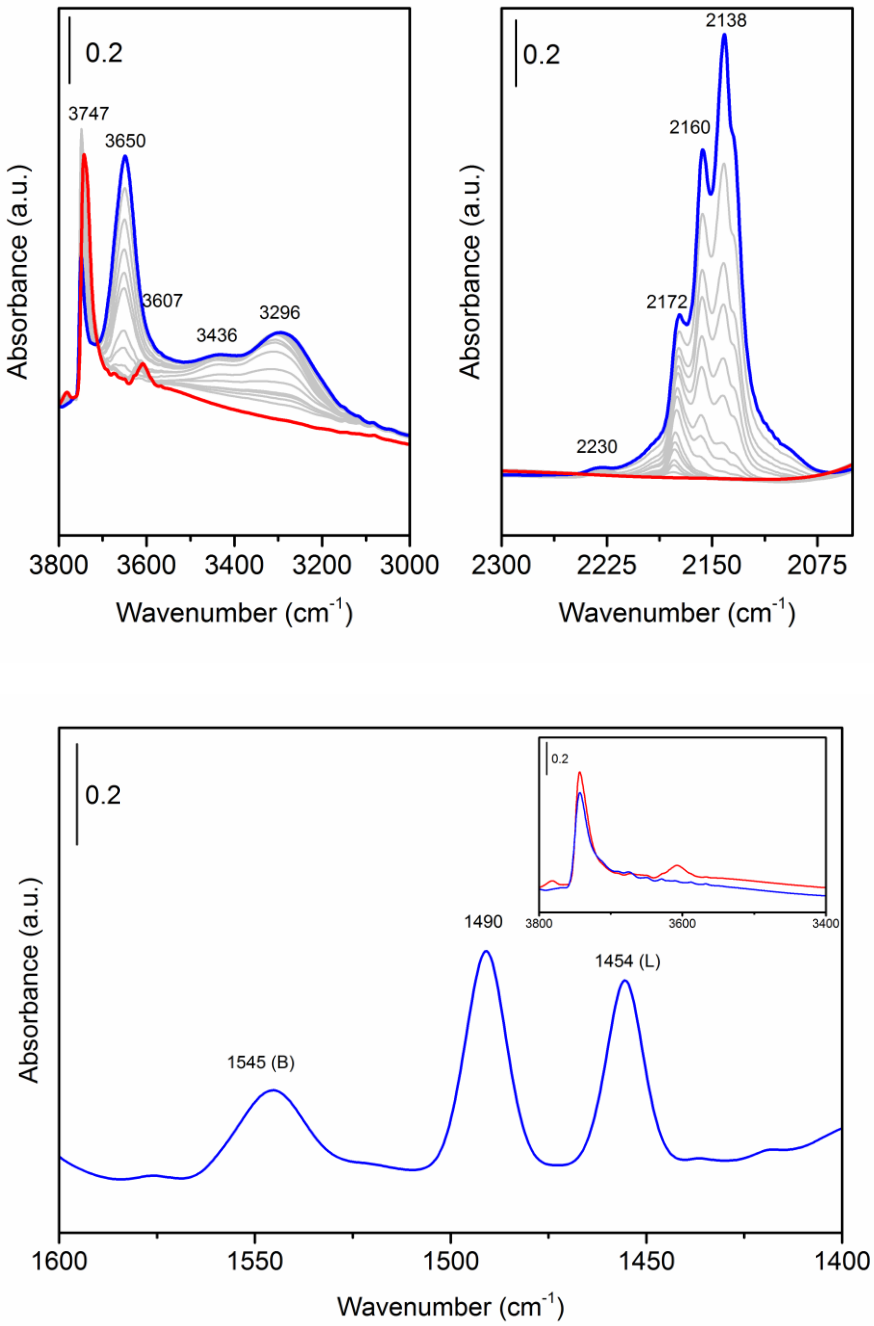


**Figure S.8.** Top: FTIR spectra of Beta zeolite upon interaction with CO in the OH region (left) and in the CO region (right). Bottom: FTIR spectra of BETA upon interaction of pyridine and subsequent heating at 200 °C for two hours.

In the case of SAPO-34, as the dimensions of the 8 membered ring channels are smaller than the kinetic diameter of pyridine, CO was the only probe molecule used. The spectrum of the dehydrated zeolite is shown in red in Figure S.9. The spectrum displays a doublet assigned to Brønsted acid sites. The high frequency vibration at 3625 $cm^{-1}$ has a higher intensity compared to the band at 3600 $cm^{-1}$. There are other bands observed at 3740 $cm^{-1}$ and 3680 $cm^{-1}$ associated to Si-OH and P-OH species as it has been previously described [12]. Upon interaction with CO, the doublet of Brønsted sites erodes and a band with the maximum at 3348 $cm^{-1}$ appears. In the CO stretching region, the polarization of CO by strong Brønsted sites is observed by the peak at 2170 $cm^{-1}$ whereas the CO physisorbed in the channels is observed at 2141 $cm^{-1}$.

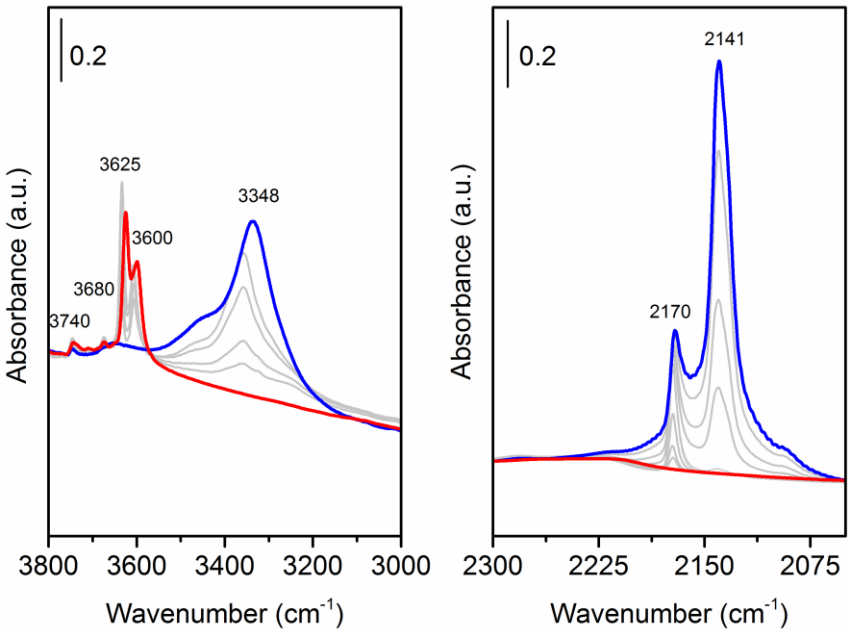


**Figure S.9.** FTIR spectra of SAPO-34 upon interaction with CO in the OH region (left) and in the CO region (right).

## S.3. Influence of pre-treatment conditions in partially deactivated catalysts on BET area

In order to measure the BET surface area on partially deactivated catalysts water has to be the only compound desorbed from the catalyst. The influence of pre-treatment conditions was investigated using four partially deactivated samples with different extent of deactivation: two completely deactivated Mordenite and ZSM-22 samples and two additional Mordenite samples which were used in the conversion of methanol to hydrocarbons for 15 and 25 minutes, respectively.

Samples were pre-treated in in a two-step procedure. First, the catalysts were outgassed for 1 hour at 80 °C followed by 3 hours treatment. In this second step samples were exposed to three different temperatures: 150, 200 and 250 °C. Results show that the BET surface area was unmodified by the temperature used of the second pre-treatment step. We chose 200 °C for the evacuation of the coked samples.

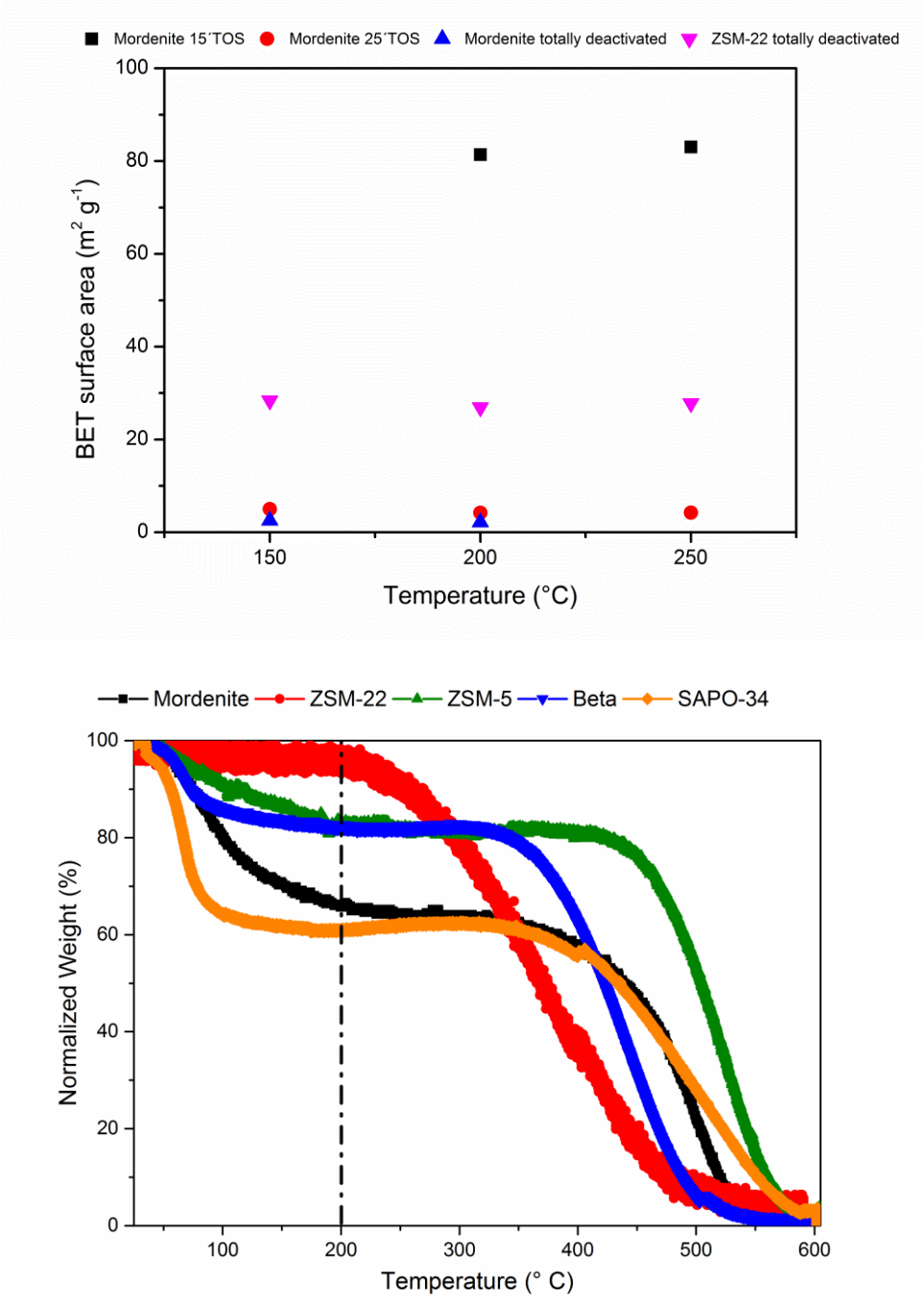


**Figure S.10.** Top-BET surface area of partially coked samples pre-treated at different temperatures. Bottom-Thermogravimetric profiles of deactivated zeolite catalysts showing that only water was removed by pretreating the samples at 200 °C

## S.4. Dissolution-extraction experiments

A calibration of the GC-MS was carried out to quantify the soluble coke species. The calibration curve is shown in Figure S.11. A mixture of 40.5 mg of xylene, 27.7 mg of naphthalene, 29.5 mg of hexamethylbenzene and 40.0 mg of phenanthrene were diluted into 50 mL of $CH_2Cl_2$ containing ortho-Cl-Toluene as internal standard. The solution was diluted four times, providing a concentration range expected to cover the amount of hydrocarbons extracted from the deactivated catalysts.

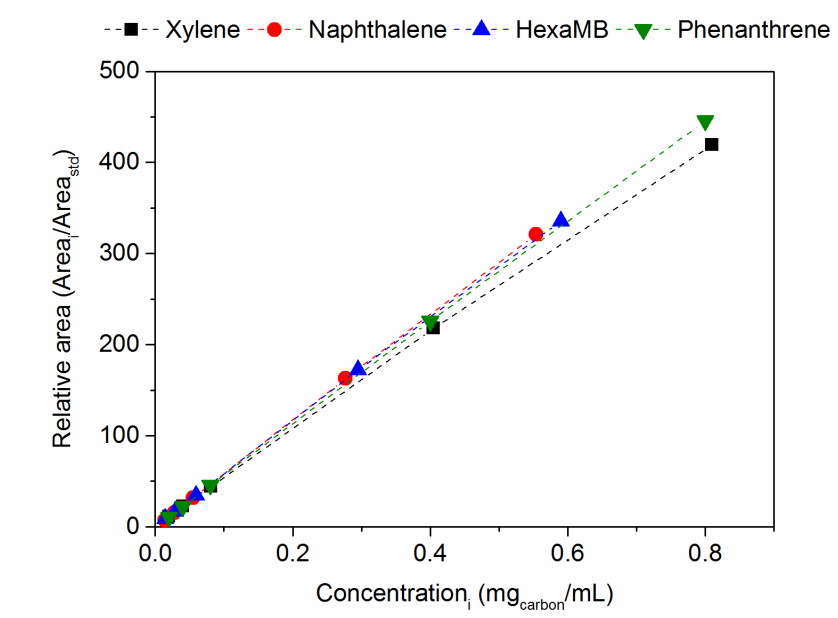


**Figure S.11.** Calibration curves for the different coke species. The concentration is given in mg of C per mL. The integrated area of each compound in the chromatogram is normalized with the area of the internal standard (o-Cl-Toluene).

It should be noted that this quantitative analysis constitutes an estimate that will be on the low side. Several issues contribute to this. First, we carry out only one extraction with organic solvent. This was done in order to minimize volumes and to avoid dilution of the extracts. Second, the acidic water phase is not neutralized, meaning that some compounds with very high proton affinity might be retained in the water phase. We decided against neutralization, as this generates heat, which in some cases leads to violent boiling in the Teflon tube. Third, very volatile retained compounds (like methanol/DMEN, species derived from surface methoxy groups, and butanes and pentanes, which will be trapped in SAPO-34) elute before or with the solvent during GC analysis and are thus also not detected.

### S.4.1 Mordenite

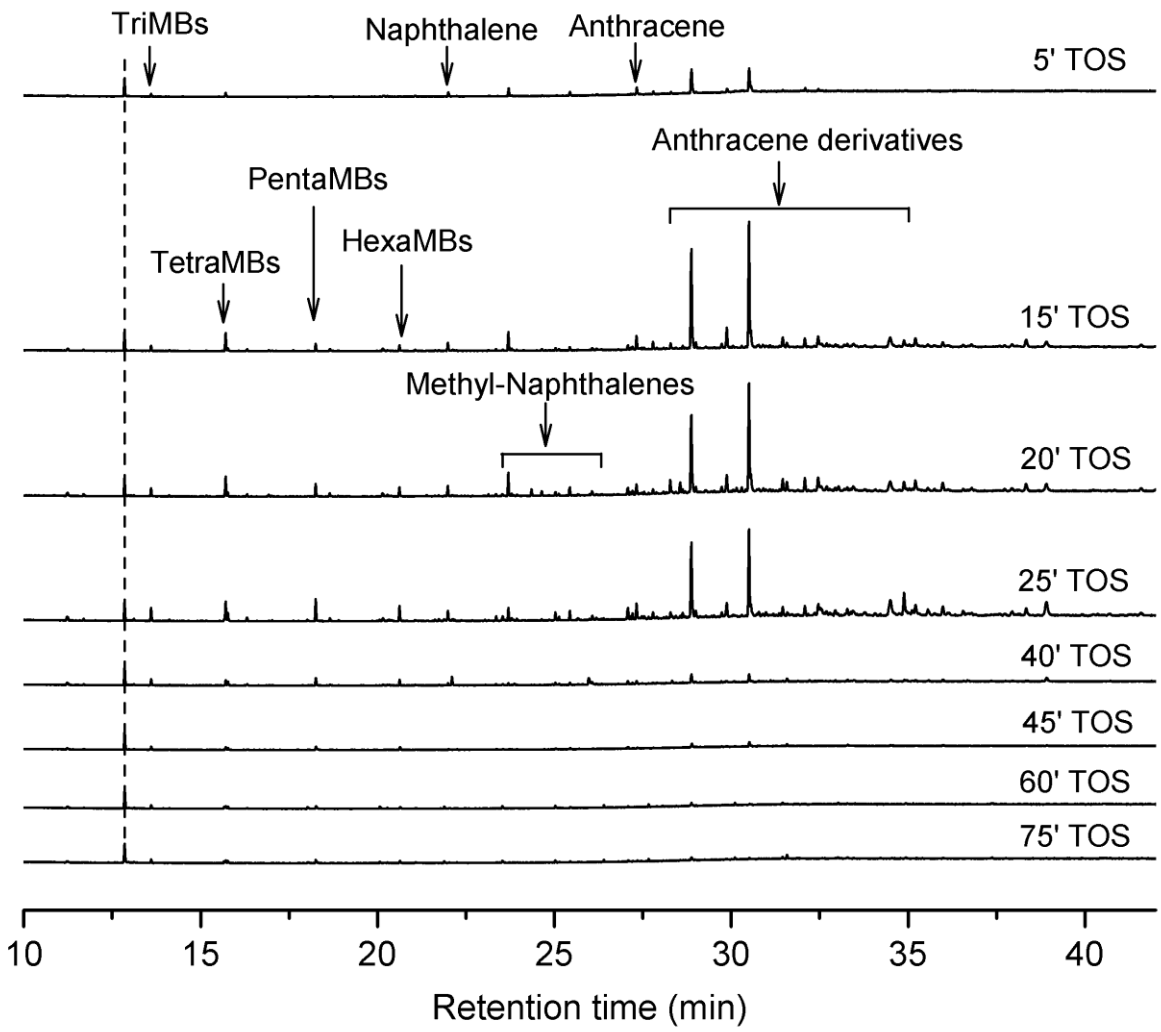


**Figure S.12.** Chromatograms showing the soluble coke compounds detected in Mordenite when the dissolution-extraction experiment was applied. Ortho-Cl-Toluene was used as internal standard and it is shown with the dotted line.

### S.4.2 ZSM-22

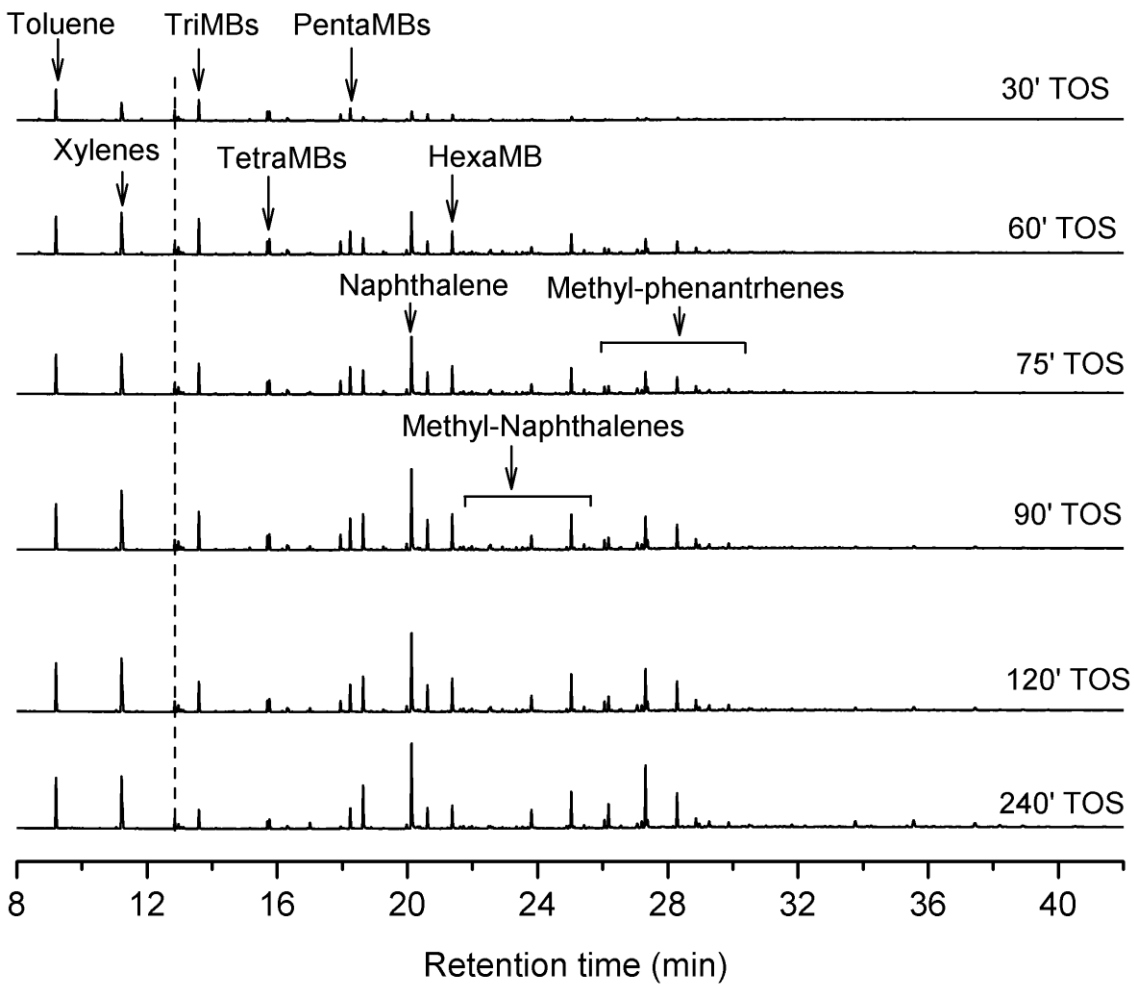


**Figure S.13** Chromatograms of the soluble coke compounds detected in ZSM-22 in dissolution-extraction experiment. Ortho-Cl-Toluene was used as internal standard and it is shown with the dotted line.

### S.4.3 ZSM-5

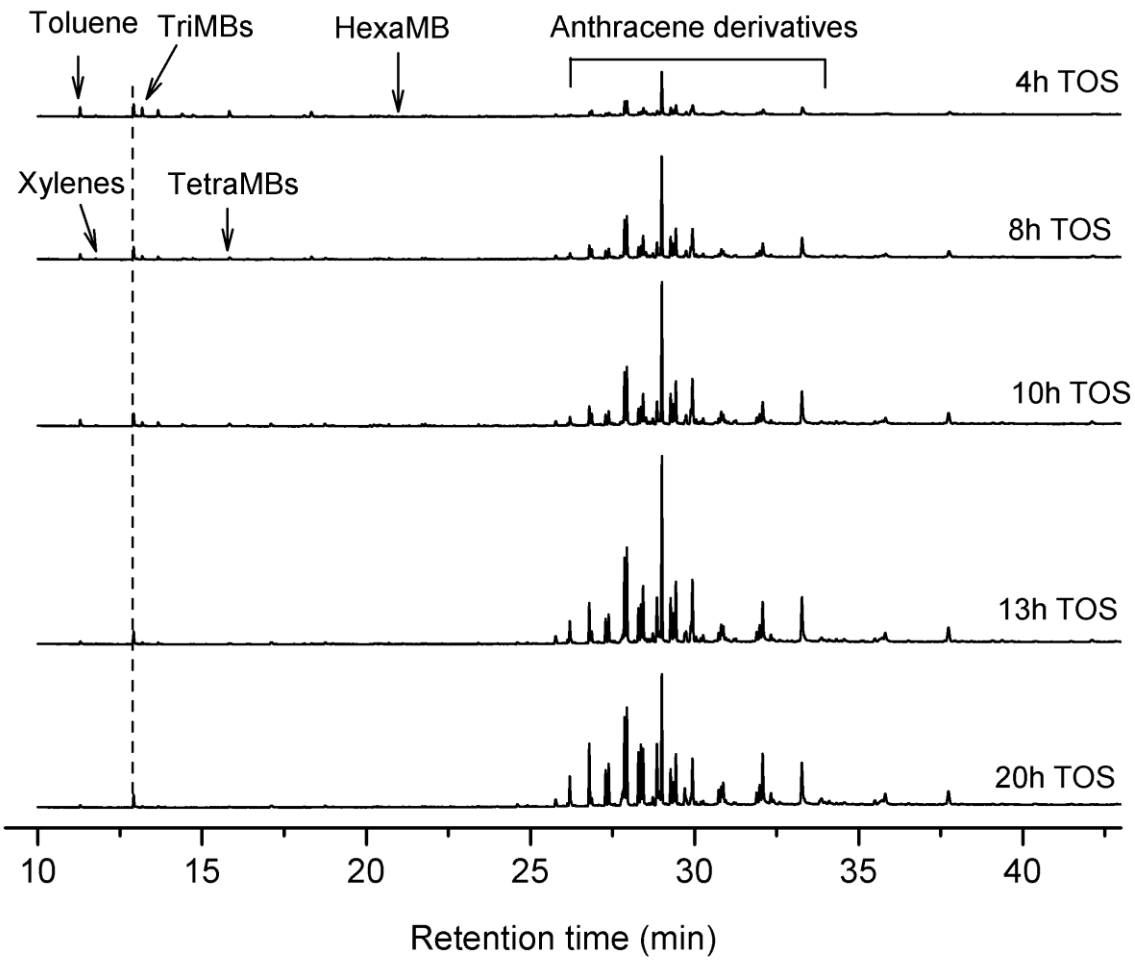


**Figure S.14** Chromatograms of the soluble coke compounds detected in ZSM-5 in dissolution-extraction experiment. Ortho-Cl-Toluene was used as internal standard and it is shown with the dotted line.

### S.4.4 BETA

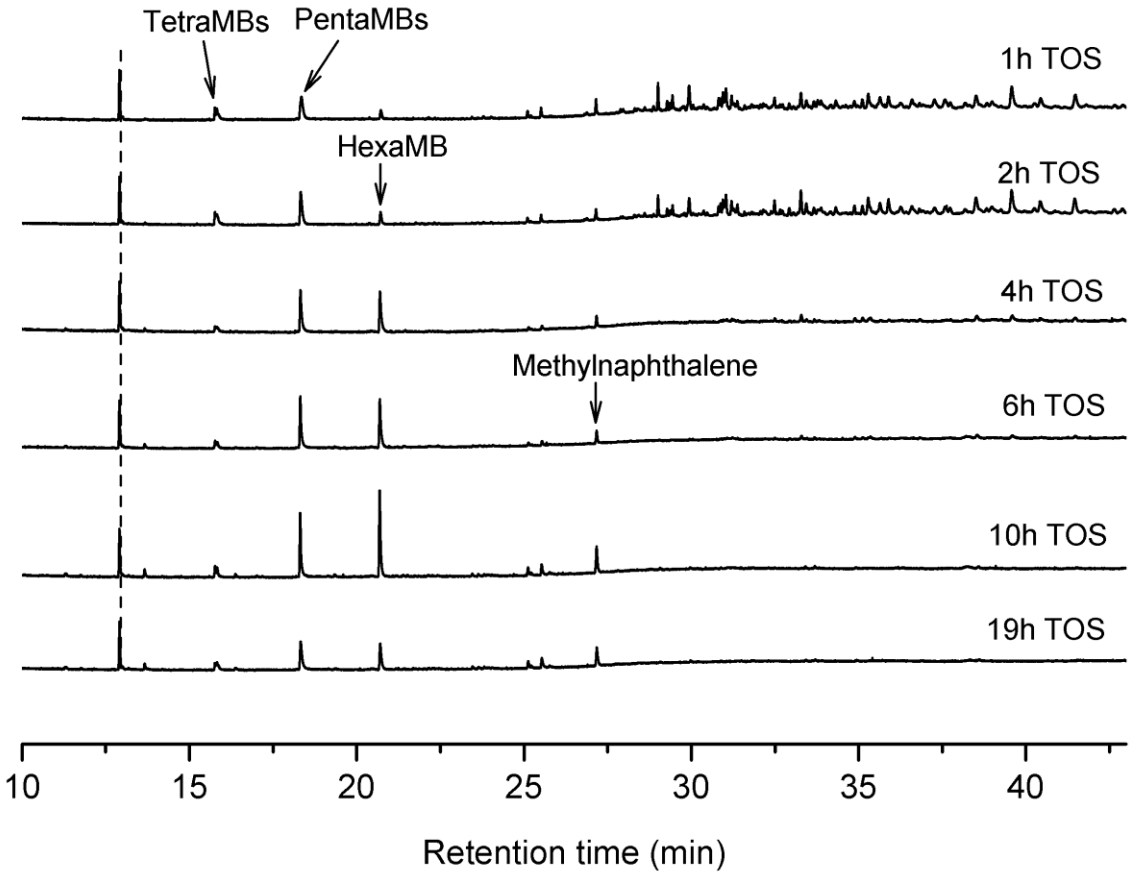


**Figure S.15** Chromatograms of the soluble coke compounds detected in BETA zeolite in dissolution-extraction experiment. Ortho-Cl-Toluene was used as internal standard and it is shown with the dotted line.

### S.4.5 SAPO-34

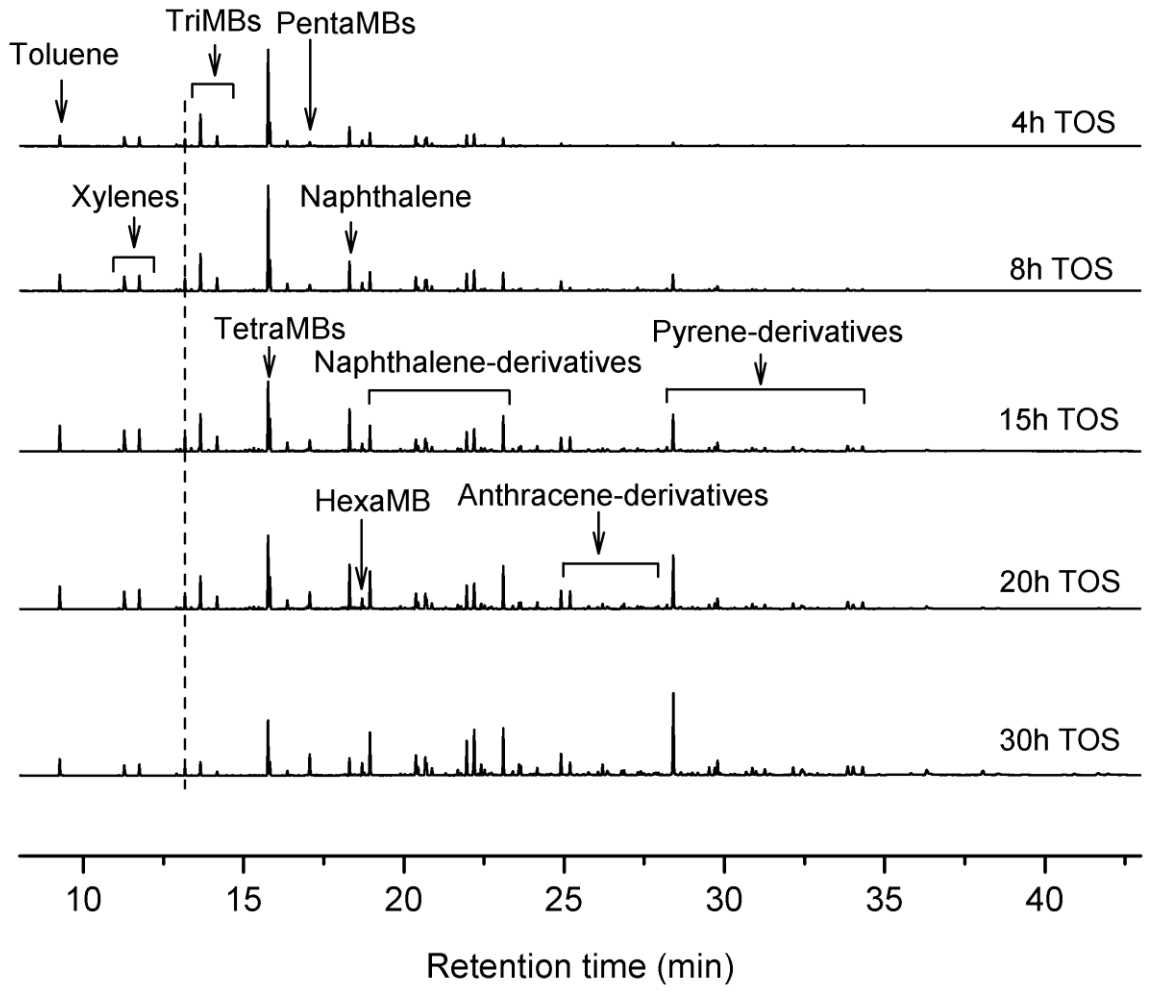


**Figure S.16** Chromatograms of the soluble coke compounds detected in SAPO-34 in dissolution-extraction experiment. Ortho-Cl-Toluene was used as internal standard and it is shown with the dotted line.

## S.5 Activity - deactivation relationships

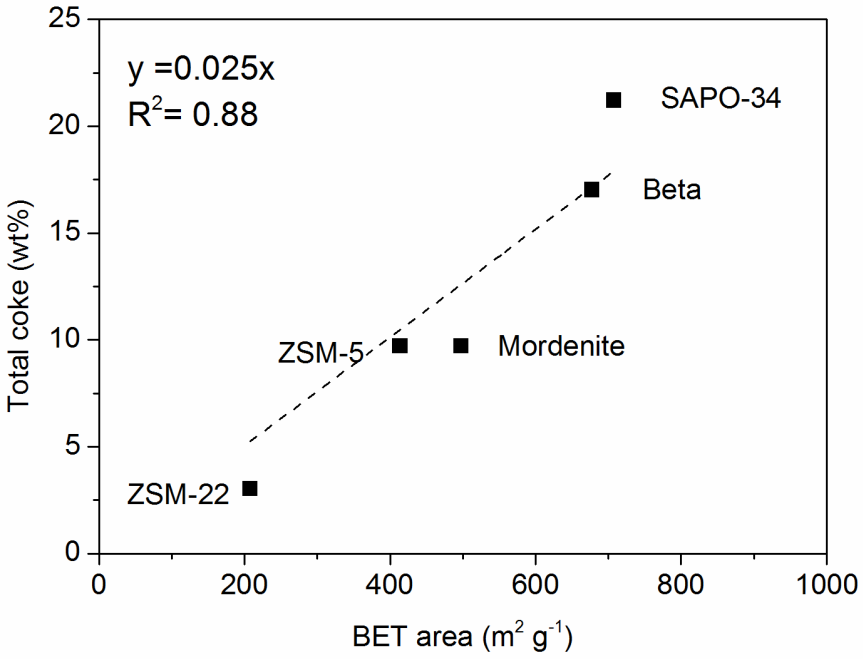


**Figure S.17.** Correlation between the coke content on totally deactivated samples and the BET area on fresh catalysts. The regression analysis is forced through the origin.

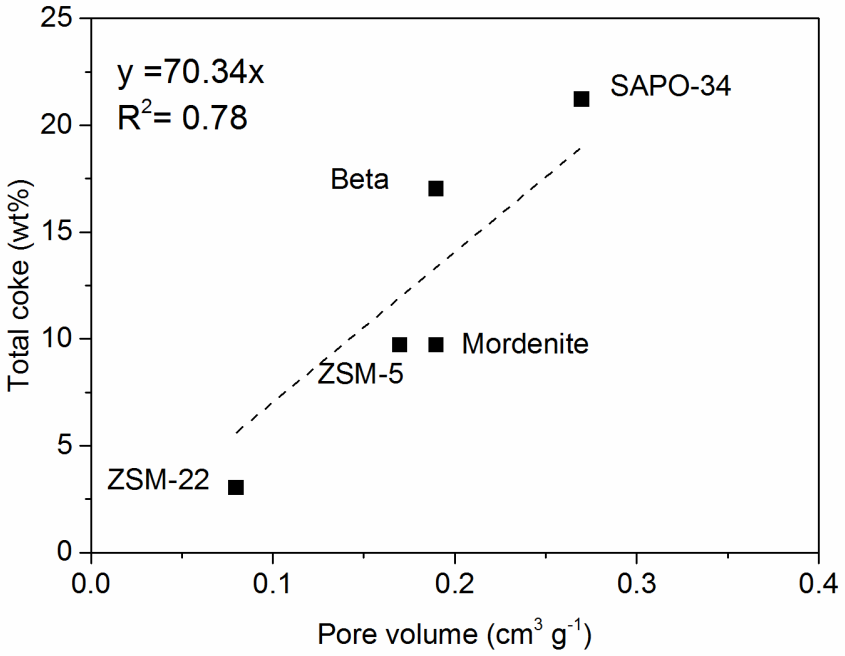


**Figure S.18.** Correlation between the coke content on totally deactivated samples and the pore volume on fresh catalysts. The regression analysis is forced through the origin.

## S.6 UV-Raman experiments

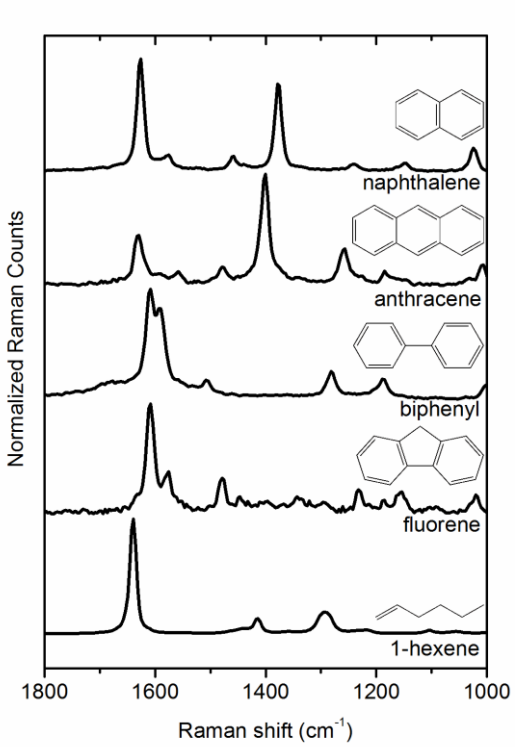


**Figure S.19.** UV-Raman (λ = 244 nm) spectra of reference deactivation compounds and their structures.

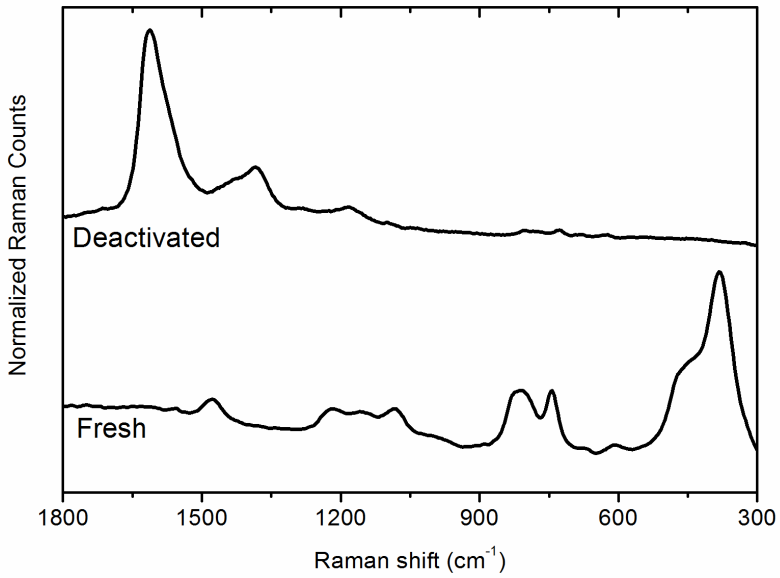


**Figure S.20.** UV-Raman (λ = 244 nm) spectrum of fresh ZSM-5 sample (i.e. after calcination) compared with the fully deactivated catalyst.

Figure S.20 compares the spectra obtained for a fresh and completely deactivated ZSM-5 catalyst. The Raman spectrum of the fresh ZSM-5 is characterized by three major band intervals: $\nu_{asym}$ (Si-O-Si) stretching modes (1200-1050 $cm^{-1}$, weak intensities), $\nu_{sym}$ (Si-O-Si) (850-700 $cm^{-1}$, medium intensities), and zeolite ring modes (500-300 $cm^{-1}$, strong intensities). Once the zeolite is deactivated, none of these bands are observable and the spectrum is dominated by contributions from the carbonaceous species.

## S.7 Additional comparisons among catalysts.

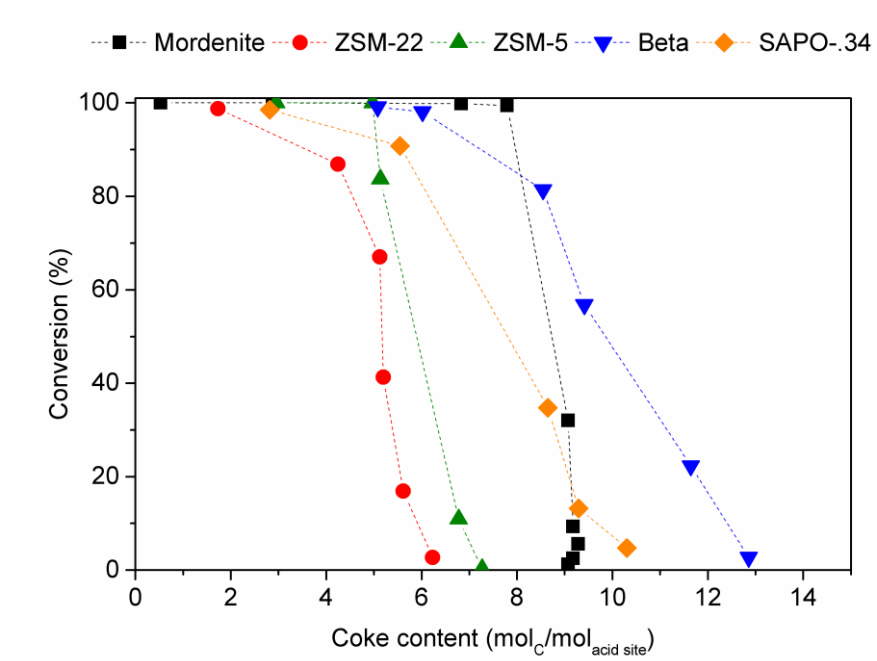


**Figure S.21. C**onversion of methanol aganst the total amount of carbon (in mols) per mol of acid site over the different catalysts.

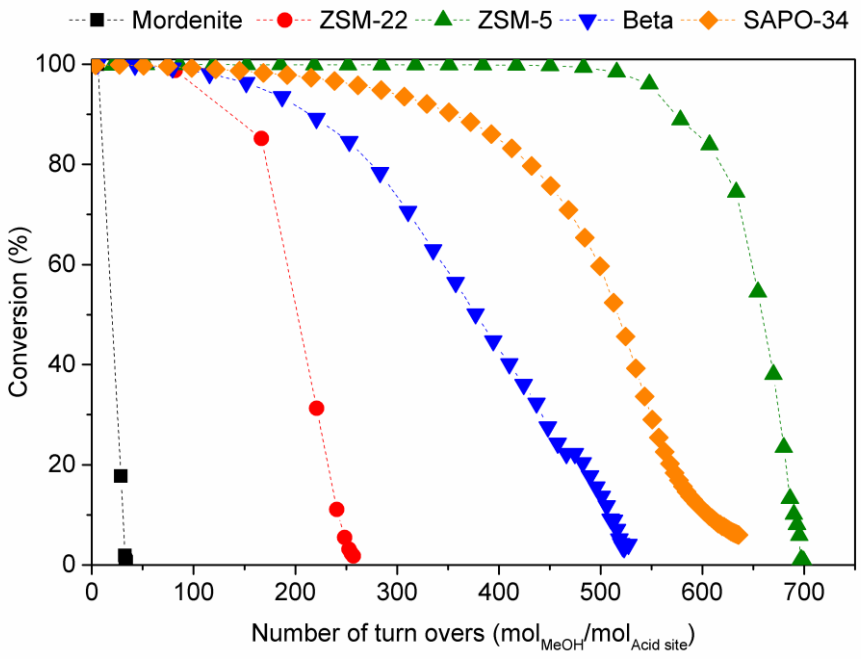


**Figure S.22.** Conversion of methanol vs the number of turnovers for the different catalysts.

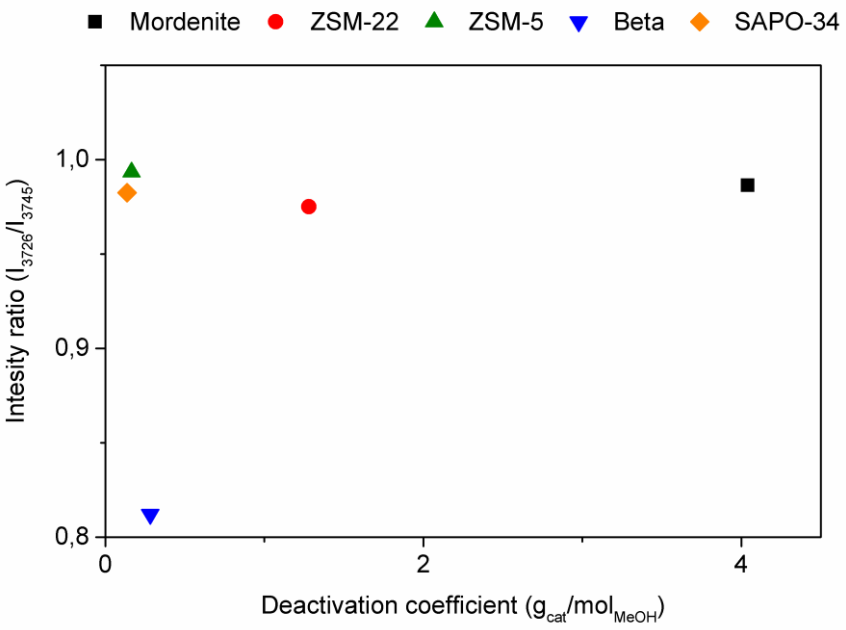


**Figure S.23**. Correlation between the IR instensity ratio ($I_{3726}/I_{3745}$) and the deactivation coefficient for the five catalysts.

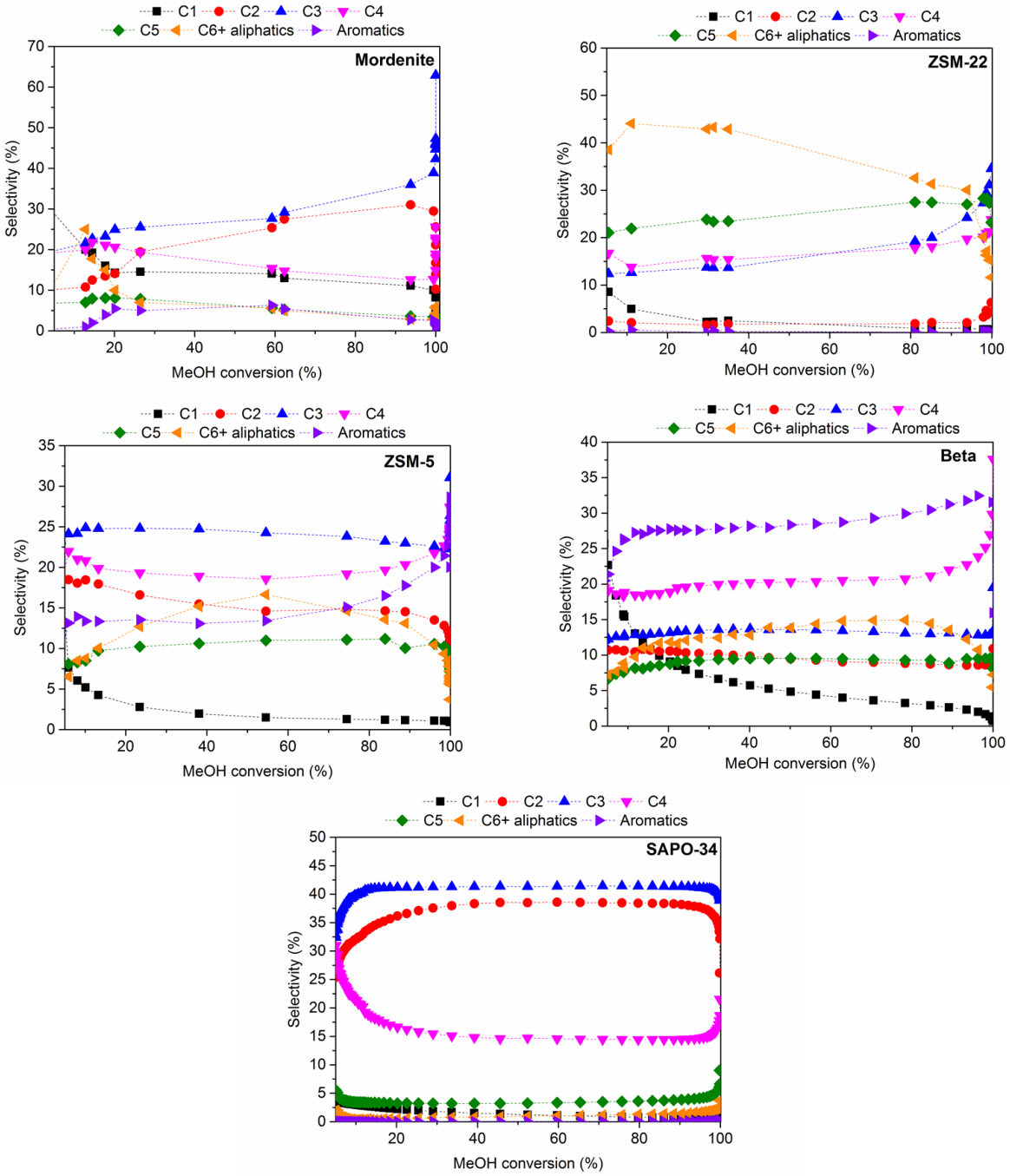


**Figure S.24** Product selectivities at increasing methanol converison for the 5 catalysts used.

## S.8 Estimation of the location of coke

By combining the experimental results from TGA and gas adsorption experiments, it is possible to estimate the amounts of coke located on the external surface and in the internal structure [13]. TGA provides the total amount of coke (internal + external) and it is assumed that the reduction in micropore volume in the partially deactivated samples relative to the fresh catalysts corresponds to the coke located in the micropores (internal coke) [14, 15] by assuming 1.22 g $cm^{-3}$ as the density of coke [15]. The external coke is found by subtraction between the total and the internal coke.

Results show that this method substantially overestimates the amount of external coke in all materials.

**Table S.3** Comparison of the total coke (TG) and the internal coke calculated from the reduction in micropore volume in the partially deactivated Mordenite samples.

| Mordenite | | |
|---|---|---|
| TOS | Total coke (mg coke / mg zeolite) | Internal coke (mg coke/mg zeolite) |
| 0 | 0 | 0 |
| 5 | 0.005 | 0.005 |
| 10 | 0.03 | 0.12 |
| 15 | 0.07 | 0.18 |
| 20 | 0.08 | 0.21 |
| 30 | 0.10 | 0.22 |
| 40 | 0.10 | 0.22 |
| 45 | 0.10 | 0.22 |
| 60 | 0.10 | 0.22 |
| 75 | 0.10 | 0.22 |

**Table S.4** Comparison of the total coke (TG) and the internal coke calculated from the reduction in micropore volume in the partially deactivated ZSM-22 samples.

| ZSM-22 | | |
|---|---|---|
| TOS | Total coke (mg coke / mg zeolite) | Internal coke (mg coke/mg zeolite) |
| 0 | 0 | 0 |
| 30 | 0.01 | 0.01 |
| 60 | 0.02 | 0.08 |
| 75 | 0.03 | 0.08 |
| 90 | 0.03 | 0.08 |
| 120 | 0.03 | 0.09 |
| 240 | 0.03 | 0.09 |

**TableS.5** Comparison of the total coke (TG) and the internal coke calculated from the reduction in micropore volume in the partially deactivated ZSM-5samples

| ZSM-5 | | |
|---|---|---|
| TOS | Total coke (mg coke / mg zeolite) | Internal coke (mg coke/mg zeolite) |
| 0 | 0 | 0 |
| 4 | 0.04 | 0.08 |
| 8 | 0.07 | 0.13 |
| 10 | 0.07 | 0.15 |
| 13 | 0.09 | 0.16 |
| 20 | 0.10 | 0.19 |

**Table S.6** Comparison of the total coke (TG) and the internal coke calculated from the reduction in micropore volume in the partially deactivated samples of Beta.

| Beta | | |
|---|---|---|
| TOS | Total coke (mg coke / mg zeolite) | Internal coke (mg coke/mg zeolite) |
| 0 | 0 | 0 |
| 1 | 0.06 | 0.10 |
| 2 | 0.07 | 0.12 |
| 4 | 0.11 | 0.17 |
| 6 | 0.12 | 0.18 |
| 10 | 0.15 | 0.21 |
| 19 | 0.17 | 0.23 |

**Table S.7** Comparison of the total coke (TG) and the internal coke calculated from the reduction in micropore volume in the partially deactivated samples of SAPO-34.

| SAPO-34 | | |
|---|---|---|
| TOS | Total coke (mg coke / mg zeolite) | Internal coke (mg coke/mg zeolite) |
| 0 | 0 | 0 |
| 4 | 0.05 | 0.20 |
| 8 | 0.11 | 0.25 |
| 15 | 0.17 | 0.32 |
| 20 | 0.19 | 0.33 |
| 30 | 0.21 | 0.33 |

# References

[1] C. Baerlocher, L.B. McCusker, D.H. Olson, Atlas of zeolite framework types, Elsevier, 2007.
[2] J.B. Higgins, R.B. LaPierre, J.L. Schlenker, A.C. Rohrman, J.D. Wood, G.T. Kerr, W.J. Rohrbaugh, The framework topology of zeolite beta, Zeolites, 8 (1988) 446-452.
[3] J.C. Groen, L.A.A. Peffer, J. Pérez-Ramírez, Pore size determination in modified micro- and mesoporous materials. Pitfalls and limitations in gas adsorption data analysis, Microporous and Mesoporous Materials, 60 (2003) 1-17.
[4] J.C. Groen, J. Pérez-Ramírez, Critical appraisal of mesopore characterization by adsorption analysis, Applied Catalysis A: General, 268 (2004) 121-125.
[5] S. Bordiga, C. Lamberti, F. Geobaldo, A. Zecchina, G.T. Palomino, C.O. Arean, Fourier-Transform Infrared Study of CO Adsorbed at 77 K on H-Mordenite and Alkali-Metal-Exchanged Mordenites, Langmuir, 11 (1995) 527-533.
[6] A. Zecchina, S. Bordiga, G. Spoto, D. Scarano, G. Petrini, G. Leofanti, M. Padovan, C.O. Arean, Low-temperature Fourier-transform infrared investigation of the interaction of CO with nanosized ZSM5 and silicalite, Journal of the Chemical Society, Faraday Transactions, 88 (1992) 2959-2969.
[7] T.K. Phung, G. Busca, On the Lewis acidity of protonic zeolites, Applied Catalysis A: General, 504 (2015) 151-157.
[8] L. Kustov, V. Kazanskii, S. Beran, L. Kubelkova, P. Jiru, Adsorption of carbon monoxide on ZSM-5 zeolites: infrared spectroscopic study and quantum-chemical calculations, Journal of Physical Chemistry, 91 (1987) 5247-5251.
[9] T. Yamamoto, T. Tanaka, T. Matsuyama, T. Funabiki, S. Yoshida, Alumina-supported rare-earth oxides characterized by acid-catalyzed reactions and spectroscopic methods, The Journal of Physical Chemistry B, 105 (2001) 1908-1916.
[10] E. Selli, L. Forni, Comparison between the surface acidity of solid catalysts determined by TPD and FTIR analysis of pre-adsorbed pyridine, Microporous and Mesoporous Materials, 31 (1999) 129-140.
[11] C. Morterra, G. Magnacca, A case study: surface chemistry and surface structure of catalytic aluminas, as studied by vibrational spectroscopy of adsorbed species, Catalysis Today, 27 (1996) 497-532.
[12] S. Bordiga, L. Regli, D. Cocina, C. Lamberti, M. Bjørgen, K.P. Lillerud, Assessing the acidity of high silica chabazite H-SSZ-13 by FTIR using CO as molecular probe: Comparison with H-SAPO-34, Journal of Physical Chemistry B, 109 (2005) 2779-2784.
[13] F.L. Bleken, K. Barbera, F. Bonino, U. Olsbye, K.P. Lillerud, S. Bordiga, P. Beato, T.V.W. Janssens, S. Svelle, Catalyst deactivation by coke formation in microporous and desilicated zeolite H-ZSM-5 during the conversion of methanol to hydrocarbons, Journal of Catalysis, 307 (2013) 62-73.
[14] M. Choi, K. Na, J. Kim, Y. Sakamoto, O. Terasaki, R. Ryoo, Stable single-unit-cell nanosheets of zeolite MFI as active and long-lived catalysts, Nature, 461 (2009) 246-249.
[15] D.M. Bibby, C.G. Pope, Sorption studies of coke deposited on ZSM-5, Journal of Catalysis, 116 (1989) 407-414.